This article has been accepted for publication in a future issue of this journal, but has not been fully edited. Content may change prior to final publication. Citation information: DOI 10.1109/TMI.2017.2740784, IEEE Transactions on Medical Imaging

Extended Lifetime *In Vivo* Pulse Stimulated Ultrasound Imaging

James Wang, Christopher V. Barback, Casey N. Ta, Joi Weeks, Natalie Gude, Robert F. Mattrey, Sarah L. Blair, William C. Trogler, Hotaik Lee, Andrew C. Kummel, *Member, IEEE*

***Abstract* – An on-demand long-lived ultrasound contrast agent that can be activated with single pulse stimulated imaging (SPSI) has been developed using hard shell liquid perfluoropentane filled silica 500 nm nanoparticles for tumor ultrasound imaging. SPSI was tested on LnCAP prostate tumor models in mice; tumor localization was observed after intravenous (IV) injection of the contrast agent. Consistent with enhanced permeability and retention, the silica nanoparticles displayed an extended imaging lifetime of 3.3 ± 1 days (mean ± standard deviation). With added tumor specific folate functionalization, the useful lifetime was extended to 12 ± 2 days; in contrast to ligand based tumor targeting, the effect of the ligands in this application is enhanced nanoparticle retention by the tumor. The current study demonstrates for the first time that IV injected functionalized silica contrast agents can be imaged with an in vivo lifetime ~500 times longer than current microbubble-based contrast agents. Such functionalized long-lived contrast agents may lead to new applications in tumor monitoring and therapy.**

***Index Terms*—Contrast Agents, Nanoparticles, Prostate, Ultrasound, Visualization**

I. Introduction

Ultrasound imaging is widely used in clinical diagnostics due to its portability, safety, and low cost [1]. Ultrasound contrast agents were initially developed to study cardiac function and abnormalities [2-7]. Injections of saline solution containing indocyanine green were discovered to result in echo clouds under ultrasound imaging that produces contrast with blood flow signals, and allows measurement of cardiac function [2, 8, 9]. The contrast echoes originated from the microbubbles present in the injected solutions [9]. As a result, microbubble based ultrasound contrast agents have been studied to optimize ultrasound backscatter and enable the imaging of capillary networks [10]. Current ultrasound contrast agents are largely based on low-solubility gases, such as perfluorocarbons (PFC) or sulfur hexafluoride gas microbubbles, encapsulated within a flexible liposomal shell made from a polymer or lipid. However, microbubble ultrasound contrast agents such as Definity® exhibit short *in vivo* imaging lifetimes due to their fragile lipid composition and gas diffusion [11]. For example, pressure gradients aid PFC gas dissolution into the surrounding bloodstream and dissipate the microbubble. Smaller microbubbles result in larger Laplace pressures that further accelerate PFC gas dissolution and cause bubble collapse [12, 13]. Additionally, bubble contraction and expansion during ultrasound exposure mechanically weakens the encapsulating lipid shell, resulting in short circulation lifetimes [12, 14, 15].

In order to increase the *in vivo* lifespan of ultrasound contrast agents, hard shell silica nanoparticles with a diameter of 500 nm have been synthesized that can be used to encapsulate PFC gas or liquid [16-19]. It is proposed that a single high intensity ultrasound pulse converts the liquid droplet within the silica nanoshell to the gas phase via acoustic droplet vaporization (ADV). Ultrasound can superheat a PFC liquid droplet that is stabilized by a surfactant shell to vaporize into a bubble 100 times larger in volume than that of the original liquid droplet[20, 21]. Apfel and Kripfgangs have reported applications of ADV in embolotherapy and drug delivery [20-24]. Shi and coworkers have encapsulated perfluorohexane (boiling point = 56 ^{o}C) in silica nanoshells as an enhancement agent for high intensity focused ultrasound (HIFU) therapy based on ADV [25]. However, ADV applications specifically for ultrasound imaging with encapsulated perfluoropentane (PFP) liquid (boiling point = 29 ^{o}C, Strem Chemicals) have only been studied in soft shell particles. For example, Sheeran *et al*. demonstrated that lipid encapsulated dodecafluorobutane nanodroplets could undergo ADV into micron sized gas phase

Resubmitted on August 5th, 2017.
This work was supported by National Institute of Health NIH under Grant 1R33CA177449, NIH-NCI-NCTC-R21T, and 1F31CA177199.
Copyright (c) 2017 IEEE. Personal use of this material is permitted. However, permission to use this material for any other purposes must be obtained from the IEEE by sending a request to pubs-permissions@ieee.org.

J Wang is with the Department of Nanoengineering at University of California, San Diego, CA, 92093 (email: jaw059@ucsd.edu)
C.V. Barback iss with the Department of Radiology, University of California, San Diego, CA, 92093 (email: cbarback@ucsd.edu)
C.N. Ta was with the Department of Electrical and Computer Engineering, University of California, San Diego, CA, 92093 (email: cnta@ucsd.edu)
J. Weeks is with the Integrated Regenerative Research Institute, San Diego State University, San Diego, 92182 (email: jweeks@ucsd.edu)
N. Gude is with the Integrated Regenerative Research Institute, San Diego State University, San Diego, 92182 (email: ngude@mail.sdsu.edu
R.F. Mattrey was with the Department of Radiology, University of California, San Diego, CA, 92093 (email: rmattrey@ucsd.edu)
S.L. Blair is with the Moores Cancer Center, University of California, San Diego, CA, 92093 (email: slblair@ucsd.edu)
W.C. Trogler is with the Department of Chemistry and Biochemistry, University of California, San Diego, CA, 92093 (email: wtrogler@ucsd.edu)
H. Lee is with the Samsung Advanced Institute of Technology, Samsung Electronics, Korea (email: hotaik1.lee@samsung.com)
A.C. Kummel is with the Department of Chemistry and Biochemistry, University of California, San Diego, CA, 92093 (akummel@ucsd.edu)

0278-0062 (c) 2017 IEEE. Personal use is permitted, but republication/redistribution requires IEEE permission. See http://www.ieee.org/publications_standards/publications/rights/index.html for more information.

This article has been accepted for publication in a future issue of this journal, but has not been fully edited. Content may change prior to final publication. Citation information: DOI 10.1109/TMI.2017.2740784, IEEE Transactions on Medical Imaging

bubbles at an ultrasound mechanical index (MI) of 1.2. This is within the FDA defined MI safety limit of 1.9 [26]. Kripfgans *et al*. demonstrated that a single element transducer could be used to stimulate ADV of albumin coated microdroplets into gas microbubbles in a flow channel *in vitro* and could be imaged with B-mode ultrasound [21]. A high frequency pulse could be used to convert acoustically transparent nanodroplets of lipid encapsulated PFP into B-mode visible microbubbles *in vivo* after intratumoral injection in mice grafted with hepatocellular carcinoma [24]; however, non-linear imaging, such as contrast pulse sequencing (CPS), was not demonstrated. Thus, current research in ADV has been primarily focused on PFC droplets within soft and flexible lipid or polymer shells, which lack the *in vivo* stability of the hard shell silica nanoshell particles.

In this study, a novel imaging platform is reported for liquid PFC filled 500 nm rigid shell silica nanoparticles using single pulse stimulated imaging (SPSI) to generate an ultrasound CPS signal that is visually comparable with commercial ultrasound contrast agents. While, conventional ultrasound contrast agents exhibit short *in vivo* lifetimes (< 30 minutes)[27, 28], liquid PFP core silica nanoshells represent the first type of on-demand ultrasound contrast agents with lifetimes that extend beyond several days of imaging time. Surface modification of the silica shell to target specific biomarkers such as folate extends the *in vivo* imaging lifetime by a factor of 4 times to 12 ± 2 days, which allow the biomarker to be injected at the time of biopsy even 1-2 weeks before surgical resection. This enables a new ultrasonic imaging modality with tumor enhancement and may permit time-dependent tumor development diagnosis and surgical guidance applications. The advantage of ADV with rigid shells is that they are chemically stable in tissue and can provide ultrasound signal when triggered. Surface functionalization increases tumor tissue retention up to several hours or even days after injection in contrast to soft shell nanoparticles with a short in-vivo lifetime under thirty minutes.

II. Materials and Methods

Materials. Tetramethyl orthosilicate (TMOS), trimethylphenylsilane (TMPheS), N-hydroxysuccinimide (NHS), folic acid and 3-aminopropyl triethoxysilane (3-APTES) were purchased from Sigma-Aldrich (St. Louis, MO). Iron (III) ethoxide was acquired from Gelest (Moorisville, PA). 500 nm spherical amino functionalized polystyrene templates were obtained from Polysciences (Warrington, PA). 1-Ethyl-3-(3-dimethylaminopropyl)carbodiimide (EDC) was purchased from Anaspec Inc. (Fremont, CA). 2-(4-Isothiocyanatobenzyl)-diehtylenetriaminepentaaccetic acid (DTPA) was purchased from Macrocyclics (Dallas, TX). $^{111}InCl_3$ was purchased from Covidien (Mansfield, MA). PFP was purchased from Strem Chemicals (Newburyport, MA). Milli-Q purified water was obtained from a Millipore SuperQ Plus Water Purification System (Billerica, MA). The 500 nm nanoshells used in this study were synthesized with methods previously developed [29].

Ultrasound imaging was performed with Siemens Sequoia 512 (Mountain View, CA) using the Acuson 15L8 transducer. Siemens proprietary CPS algorithm was used for contrast enhanced ultrasound imaging (CEUS). The specific ultrasound imaging parameter, such as frequency, was optimized at 7 MHz. This has been previously shown to generate highest signal to noise ratio when imaging the nanoshells as a function of ultrasound frequencies between 7 MHz to 14 MHz [17, 29]. Since the nanoshells generate the strongest signal at 7 MHz, the present studies were all performed at this frequency. An H-102 single element high intensity focused ultrasound (HIFU) transducer from Sonic Concepts (Bothell, WA) operating at 1.1 MHz was coupled with an amplifier (T&C Power Conversion Inc. Rochester, NY) and connected to a PC to generate the single high intensity pulse at 2% duty cycle for SPSI based ultrasound imaging. A waveform editor program (National Instruments, Austin, TX) was used to control the output power of the HIFU and to generate the waveform of the ultrasound pulse.

Animals and Tumor Model. SHO mice were purchased from UCSD and housed in an institutional animal care and use committee (IACUC) approved vivarium. The human prostate adenocarcinoma cell line LnCAP [30] was cultured and injected subcutaneously into the right flank of the mice. The tumors grew to 600-800 mm^3 before particle injection and ultrasound imaging. The tumor dimensions were measured with a digital caliper from VWR (Radnor, PA) and ranges from 8 mm to 16 mm on average. The tumor volumes were calculated from the dimensions using the formula $V = W \times W \times H/2$ (W is width and H is height) [31, 32]. During the injection and imaging, the mice were anesthetized with isoflurane gas and euthanized by CO_2 asphyxiation followed by cervical dislocation after experimentation. Two cohorts each with four mice were included to determine the effectiveness of folate functionalization. One cohort received injections of particles without folate functionalization while the other cohort received injections of particles with folate functionalization. All animal procedures were approved by UCSD IACUC.

In Vitro Nanoshell Ultrasound Characterization. Iron (III) doped 500 nm nanoshells were initially filled with gas or liquid PFP and suspended in degassed water at a concentration of 4 mg/mL. The nanoshells were subjected to a combination of vortex mixing and bath sonication for particle dispersion. 100 µl of the 4 mg/mL PFP filled nanoshells were suspended in 900 µl of water in an ultrasound transparent pipette bulb to mimic the dose used for *in vivo* intravenous injections. The pipette bulbs containing the nanoshells were submerged in a water bath at 37 ºC and imaged with the 15L8 ultrasound transducer at a center frequency of 7 MHz. In order to study the phase transition characteristics of liquid PFP filled nanoshells, the imaging ultrasound power was increased from low MI (0.06) to the FDA allowed *in vivo* maximum MI (1.9) for humans, which corresponds to 5.03 MPa [33]. The CPS signal response was captured on the Siemens Sequoia 512 and exported as a DICOM file for further image brightness analysis using MATLAB. A MATLAB script was written to automatically quantify the image brightness through frames of interest in the

0278-0062 (c) 2017 IEEE. Personal use is permitted, but republication/redistribution requires IEEE permission. See http://www.ieee.org/publications_standards/publications/rights/index.html for more information.

This article has been accepted for publication in a future issue of this journal, but has not been fully edited. Content may change prior to final publication. Citation information: DOI 10.1109/TMI.2017.2740784, IEEE Transactions on Medical Imaging

DICOM file and distinguish between ultrasound signal from particles and from animal movement.

In Vivo Nanoshell Biodistribution. Nanoshell radiolabeling for biodistribution was performed with a previously developed method [34]. Briefly, 4 mg of Iron (III) doped 500 nm nanoshells were incubated with 0.01% v/v 3-APTES in 1 mL ethanol for 5 hours. After removing the unreacted 3-APTES and re-suspended in 1 mL DMSO, 25% w/w folate was initially activated with EDC/NHS and incubated with the nanoshells in DMSO for 12 – 20 hours. Excess unreacted folate was removed by centrifugation and washed 3 times with DMSO. 10% v/v 3-APTES was incubated with the folate functionalized nanoshells in 1 mL ethanol for 5 hours and excess 3-APTES was removed by washing with DMSO and centrifugation for 3 times. 0.0001% DTPA was subsequently incubated with the nanoshells for 12 – 20 hours in DMSO. The folate-DTPA functionalized nanoshells were purified by washing once with DMSO and twice with ethanol by centrifugation. The folate functionalization step was omitted for nanoshells used in experiments without folate modification. The folate-DTPA and DTPA functionalized nanoshells were suspended in milli-Q water at 4 mg/mL concentration and incubated with 100 µC of $^{111}InCl_3$ for 1 hour with continuous mixing. The ^{111}In chelated nanoshells were purified with centrifugation and monitored with a Geiger counter. 100 µL of the radiolabeled nanoshells at 4 mg/mL were injected into SHO mice via the tail vein. The mice were euthanized per IACUC protocol and anatomized after 5 days. The radioactivity in the organs was measured with a Beckman gamma counter.

In Vivo Nanoshell Tumor Targeting with Folate. Three groups of four SHO mice, each grafted with LnCAP prostate tumors, were used to determine *in vivo* nanoshell passive targeting with the enhanced permeability and retention (EPR) effect and subsequent SPSI capability. Definity®, gas PFP filled nanoshells, and liquid PFP filled nanoshells were each tested on four mice for comparison. When the tumors reached 600 - 800 mm^3 in volume, 100 ul intravenous (IV) injections of 4 mg/mL liquid PFP filled nanoshells were administered through the tail vein. Before IV injection, the liquid PFP filled nanoshells were dispersed with a combination of low frequency (40 KHz) sonication and vortex mixing for 30 seconds. To minimize ADV from occurring, the nanoshells were only intermittently submerged in the bath sonicator for less than 3 seconds with the remaining time vortex mixed. Due to the difference in refractive index between PFP and water, it can be easily observed visually if the particles are filled with water or PFP. CPS and B-mode ultrasound imaging was employed to image tumors at an MI of 1.9, with a frequency of 7 MHz, 15 minutes after initial IV injection and every 24 hours thereafter until no CPS signal can be observed. A single high intensity ultrasound pulse at 1.1 MHz with a peak negative pressure of 3.5 MPa was applied directly at the LnCAP tumor for 20 µs to activate the nanoparticles before each imaging event. The entire tumor is scanned for triggered CPS signal events. The ultrasound imaging and high intensity focused ultrasound pulse experimental setup follow procedures that were previously developed and reported [17, 35]

In Vitro Cell Studies. LnCaP cells were cultured in RPMI with 10% FBS and 1% penicillin/streptomycin at 37°C, 5% CO_2 in a humidified incubator. For imaging nanoshell localization in cells, LnCaP cells were plated at a density of 5 x 10^4 cells/well in Lab-Tek II 4-well chamber slides. Six samples of cells where grown for a total of 6 days. In addition to the control, the 5 day (5D) sample began nanoshell (NS) treatment on the second day, the 4 day (4D) sample began treatment on the third day, and so on in order to allow for synchronized sample collection. Rhodamine (RITC) labeled nanoshells with or without folate were added to cells at a concentration of 30 µg/mL per well. Samples were fixed with 4% paraformaldehyde (PFA) for 30 min, permeabilized for 4 min with 0.1% Triton X, blocked with 10% Horse Serum and stained for a 680 nm conjugated Wheat germ agglutinin (WGA) at 1:100 (Thermo Fisher Scientific, W-32465). Late endosomes were stained with a polyclonal Rab-7 primary antibody at 1:100 (Thermo Fisher Scientific, PA5-23138) followed by secondary Alexa488 conjugated antibody staining at 1:200 (Thermo Fisher Scientific, A-21206). Images were obtained using a 63x water objective on a SP8 Leica Confocal Microscope.

Aggregate Size Distribution Analysis. Z-stacks were collected by confocal microscopy and single images showing an internal slice of the cells were chosen for further analysis. The cell membrane was defined using a 5-pixel brush in GIMP software guided by a max projection of the WGA staining ranging from two z-slices above and two below the selected section. Masks were created to show nanoparticles inside the cells, on the membrane and exported for analysis in ImageJ. The number of nanoparticles was determined using area measurements created from the intensity of the nanoparticles using Threshold and Analyze particles in ImageJ. The area measurements were divided by the area of one particle (πr^2) to determine the number of particles within an aggregate event. The number of nanoparticles per event were organized into groups to create a frequency distribution. All aggregates smaller than 6 nanoshells were placed in the small group while all events larger than 6 nanoshells were collected into the large group. Aggregates smaller than 6 nanoshells were chosen for the small group because at one hour, most particles were in this group, allowing for any increase in particle aggregate size to reside in the larger group. Additionally, when considering the size of the aggregates over time after 1hr, half of the total of particle aggregates still reside in the 6 or smaller group. This allows for the split in the size of the particle aggregates to be at 6. This analysis was repeated for time points ranging from 1 hr to 120 hrs for both the RITC only and RITC-FOL nanoshell treatments.

III. Results and Discussion

Material Characterization. In vitro ultrasound experiments were performed to characterize the silica nanoshells. Scanning electron microscopy (SEM) was used to verify the spherical structure of the nanoparticles (Figure 1.) Based on transmission electron microscopy (TEM), the particles exhibit a mean diameter of 411 ± 17 nm. The *in vitro* CPS ultrasound at MI= 1.9 and color Doppler signal demonstrated that the silica

0278-0062 (c) 2017 IEEE. Personal use is permitted, but republication/redistribution requires IEEE permission. See http://www.ieee.org/publications_standards/publications/rights/index.html for more information.

This article has been accepted for publication in a future issue of this journal, but has not been fully edited. Content may change prior to final publication. Citation information: DOI 10.1109/TMI.2017.2740784, IEEE Transactions on Medical Imaging

nanoparticles were suitable for imaging based on the strong CPS contrast and color Doppler signals (Figure 1.) Under high mechanical index (1.9) ultrasound power insonation, a large population of nanoshells are simultaneously imaged. The high reflectivity of the nanoshells results in a significant degree of color Doppler shadowing that is characteristic of a long Doppler tail [34].

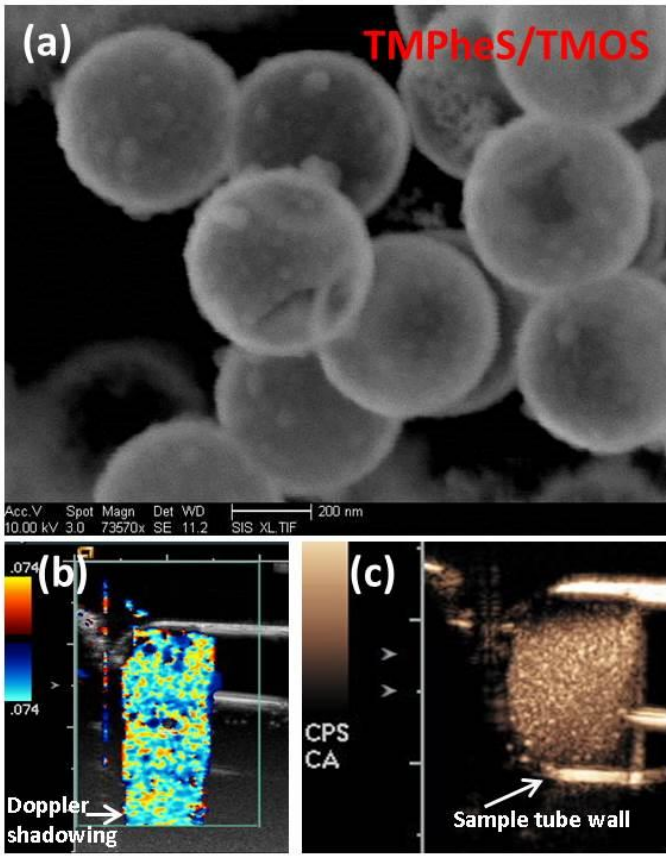

Figure 1. Silica nanoparticle characterization and performance. (a) SEM images (b) Color Doppler imaging (c) CPS imaging.

Murine Tumor In Vivo Ultrasound Imaging. In contrast to microbubbles, the rigidity of the calcined silica nanoshells results in long-term *in vivo* stability that offers long-term image guidance and tumor detection. In contrast to soft shell encapsulated PFP, the nanoshell particles are small enough to exhibit the enhanced permeability and retention (EPR) effect to passively accumulate in leaky tumor vasculature and become retained as demonstrated in previous work [34]. Hashizume *et al* have demonstrated that the endothelial walls of leaky vasculatures in tumors have pore openings up to 2 μm in diameter originating from poorly connected, branched lining cells [36]. Danquah *et al* also found that tumor vessels had endothelial openings from 0.1 to 3 μm [37, 38]. Similarly, Yuan *et al* have found that the pore cutoff size ranges between 400 – 600 nm and Hobbs *et al* mentioned that the pore cutoff size of most tumors ranges from 380 – 780 nm [39, 40]. As a result, 500 nm nanoshells may likely migrate through tumor endothelial pore openings that are large enough for extravasation and accumulation. Conventional lipid or polymer shell based microbubbles are short-lived and cannot be used for ultrasound imaging after several minutes[27, 28]. Thus, microbubbles are usually used for tumor vascular blood flow studies based on real-time vascular perfusion.

Figure 2 (a) illustrates the ability of the silica nanoshells to accumulate at the tumor site, which is attributed to the EPR effect. After initial IV tail vein injection in the SHO mice grafted with LnCAP prostate adenocarcinoma, the mice were imaged daily with ultrasound CPS imaging and SPSI mode (Figure 2 (a)).

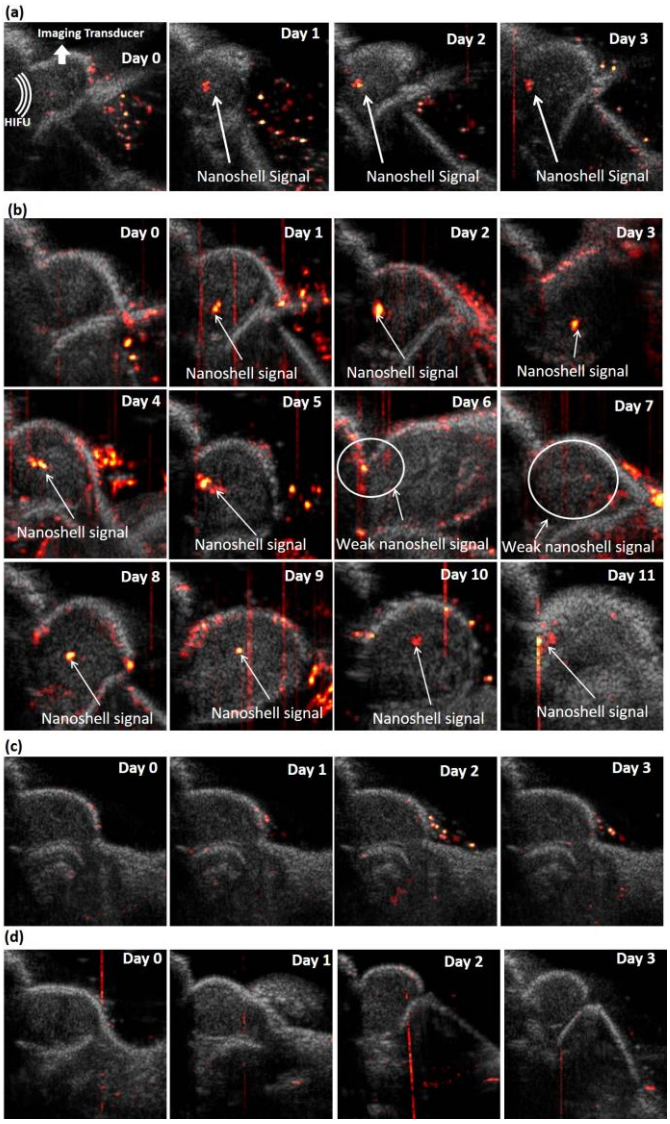

Figure 2. Representative stimulated CPS of nanoparticles in tumor over time. The CPS signal was detected 20 μs after the HIFU pulse (a) Without folate functionalization (b) After folate functionalization. (c) Control experiment with injected with nanoshells but without HIFU pulse stimulation (d) Control experiment with no nanoshell injection and stimulated with HIFU pulse

It has been demonstrated in previous work that IV injected radiolabeled nanoshells accumulate in the tumor, as well as the liver [34]. Thus, the nanoshells were expected to accumulate at the tumor site after IV administration in the present study. The mice were imaged with CPS and SPSI ultrasound daily after the initial injection. Figure 2 (a) shows that when a single high intensity ultrasound pulse is delivered to the tumor, the particles

0278-0062 (c) 2017 IEEE. Personal use is permitted, but republication/redistribution requires IEEE permission. See http://www.ieee.org/publications_standards/publications/rights/index.html for more information.

This article has been accepted for publication in a future issue of this journal, but has not been fully edited. Content may change prior to final publication. Citation information: DOI 10.1109/TMI.2017.2740784, IEEE Transactions on Medical Imaging

can be activated and imaged by CPS ultrasound imaging. The signal lifetime after each high intensity ultrasound pulse lasts for 1 second (Supplementary Figure 5). Note this is a different measurement than continuous HIFU induced imaging at a single spot which last over 5 minutes *in vivo*. Without the triggering ultrasound pulse, however, the particles remain dormant and do not interfere with traditional ultrasound CPS ultrasound tissue imaging. In contrast, tumors without nanoshells injection do not exhibit any CPS signal under pulse stimulation (Figure 2(d)). Furthermore, control experiments with injected nanoshells but no HIFU pulse, and no nanoshells but with HIFU pulse throughout a period of 2 weeks have shown no CPS signal from the tumor (Supplementary Figure 7). Since each HIFU pulse has a duration of 20 μs, animal movement before and after the pulse can be negligible. However, because the mouse tumor cross-section is manually placed at the beam intersection of the ultrasound transducer and HIFU transducer, precise 3-D placement of is achieved but reposition at the same exact cross-section between daily timepoints is difficult. Note that stimulated CPS signal appears to be localized within the tumor. This is consistent with elevated tumor center interstitial pressure and low tumor peripheral pressure that results in localized distribution of nanoparticles in the tumor [41-43]. Additionally, SPSI requires that the nanoparticle and imaging transducer maintain alignment for the stimulated CPS signal to be detected, thereby limiting the CPS signal generation events. Supplemental Figure 6 shows an example where tumor with accumulated nanoshells was stimulated with high intensity pulse at two different locations to generate CPS signal. The particles accumulate in the tumor site, remain stationary, and can be imaged for a mean of 3.3 ± 1 days as observed by SPSI. Figure 2 (a) is a representative image of a mouse over 3 days, which was taken from the cohort of 4 mice injected with non-functionalized nanoshells. The liquid PFP filled nanoshells still displayed strong CPS signals 3 days after initial IV injection. In contrast, conventional gas filled lipid or polymer based ultrasound contrast agents exhibit an imaging lifetime of less than 30 minutes [27, 28].

With EPR and active folate functionalization towards PSMA, which is up-regulated in the LnCAP tumor, the silica nanoparticle *in vivo* lifetime in the tumor is extended to a mean of 12 ± 2 days as detectable via SPSI (Fig 2 (b) and Fig 3). This significantly exceeds the 3.3 day imaging lifetime (Fig 3) when particle accumulation was based solely on the EPR effect. Figure 2 (b) is an 11 day representative image of a mouse from the cohort of 4 mice that received functionalized nanoshell injections. It can be seen with CPS that the folate functionalized nanoshells were stably localized within the LnCAP tumor. PSMA in LnCAP tumors has been shown to exhibit folate hydrolase activity which mediates the cellular uptake of folate conjugated nanoparticles [44-46]. Alternatively, activated macrophages could act as an ultrasound contrast carrier directed towards locally inflamed tissue. Inflammatory signals stimulate macrophages to express folate receptors and can also mediate internalization of folate-linked molecules [47, 48]. Wong *et al* has further demonstrated that LnCAP cells activate and recruits macrophages via NFκB activation [49]. An alternative hypothesis is that folate functionalized silica nanoshells could be internalized by activated macrophages that express folate receptors and then transported to the LnCAP tumor site or are better retained in the LnCAP tumor site by macrophages in the tumor.

To further quantify the CPS signal, particle average CPS image brightness decay over time has been characterized to compare the ultrasound *in vivo* lifetime between folate functionalized and non-functionalized nanoshells. A total of 12 mice with 4 mice for each group (folate functionalized nanoshells, non-folate functionalized nanoshells, no nanoshell injection) were analyzed for their CPS signal brightness with MATLAB. The CPS signal average brightness over time with standard deviation was ploted in Figure 3. It is found that after nanoshell injection, the particle begins to accumulate within the tumor and reaches maximum image brightness at the second day, which corresponds to maximum particle accumulation in the tumor. *In vitro* experiments have shown that higher particle concentrations result in higher image brightness. Non-functionalized nanoshells began to slowly wash out over day 3 and 4. Starting from day 5, no signal could be observed in any mice injected with non-functionalized nanoshells. In contrast, functionalized nanoshells displayed an extended *in vivo* signal for a mean of 12 ± 2 days. Since an interstitial pressure gradient exists from the tumor core decreasing towards the tumor periphery, non-functionalized nanoshells may wash out of the tumor [50]. Tumor specific targeting may increase the nanoshell retention within the tumor tissue, thereby lengthening the *in vivo* imaging time. Functionalization is often thought to have minimal effect in delivering large nanoparticles to tumors[51]; however, here the effect of functionalization is significant. This is attributed to enhanced nanoparticle retention by the tumor after escape from the vasculature. The decrease in image brightness over 12 days for the folate nanoshells is consistent with the combined results of slow PFP diffusion into surrounding tissue, and particle exhaustion due to the daily application of pulsed imaging. There is a considerable amount of noise in the signal decay over time that may be attributed to mouse movement and the variance in relative imaging location. The similarity in maximum image brightness observed on the 2nd day (Fig 3.) between the folate-functionalized and non-functionalized particles suggests that folate-functionalization does not increase accumulated particle concentration within the tumor. While EPR appears to be the dominant targeting mechanism, folate functionalization promotes an extended tumor retention time and resulting imaging longevity.

0278-0062 (c) 2017 IEEE. Personal use is permitted, but republication/redistribution requires IEEE permission. See http://www.ieee.org/publications_standards/publications/rights/index.html for more information.

This article has been accepted for publication in a future issue of this journal, but has not been fully edited. Content may change prior to final publication. Citation information: DOI 10.1109/TMI.2017.2740784, IEEE Transactions on Medical Imaging

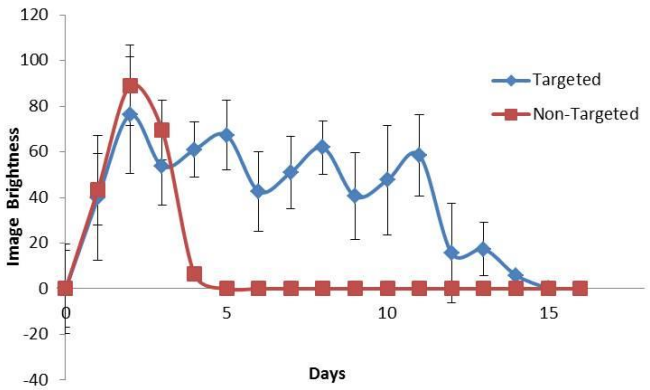

Figure 3. Image brightness of functionalized particles and non-functionalized particles in mice measured over time. The error bars represent standard deviations. The standard deviations include the variability of placing and aiming the HIFU and imaging transducer with respect to each other as well as to the tumor

In Vivo Biodistribution. To further explore how the injected nanoshells accumulate within the tumor, nanoshells were radiolabeled with In^{111} via DTPA surface conjugation and IV injected into mice through the tail vein. Mice were euthanized and anatomized for single organ gamma scintigraphy measurement (Figure 4) on day 5 where the ultrasound image signal for non-functionalized nanoshells have completely diminished (Figure 3). To account for different organ and tumor weights, the scintigraphy counts were normalized to the tissue weights and total injection amount for percent injection per gram. The biodistribution histogram show 1.92 times increase in tumor retention percentage for the functionalized nanoshells compared to non-functionalized nanoshells at day 5 (2.28% ± 0.43% vs 1.19% ± 0.52%). The detected In^{111} signal from the tumor further confirms that nanoshells are present in the tumor and can be stimulated for producing a CPS signal using a high intensity ultrasound pulse.

The large splenic and liver accumulation is attributed to macrophage phagocytosis and has been found in other studies on nanoparticle biodistributions [52]. Weissleder has shown that nanoparticles ranging from 10 – 300 nm exhibits large liver and splenic accumulations while particles larger than 1000 nm accumulates in the lung [52]. Similarly, Kumar showed that synthesized organically modified silica particles at 20 nm appear to accumulate mainly within the spleen after IV injection [53]. Xie has further shown that 20 nm silica nanoparticles accumulate within the liver (30.31%) and spleen (27.32%) 7 days after IV injection [54]. Their tissue histological analysis confirmed that the liver and splenic accumulation is due to macrophage phagocytosis [54]. Godin found that 600 nm porous silicon discs mainly accumulate within the liver, yet 1700 nm porous silicon discs showed increased amounts of accumulation within the spleen [55]. Immunohistochemical analysis demonstrates a higher association with macrophages [55]. Our nanoshells are 500 nm, Fe (III) doped silica nanoparticles that are biodegradable via the Transferrin-Fe (III) chelating mechanism and fall within the size range for large liver and splenic accumulation due to macrophage phagocytosis. Furthermore, the biodistribution profile would be affected by nanoshell surface charge and tumor type that modulates macrophage quantity within the tumor stroma [52, 53, 56]. It is acknowledged that the biodistribution may be distorted somewhat by the amount of radiolabel that detaches from the surface of the nanoshell [34]. Additionally, our previous toxicology studies have shown that the nanoshells are cleared from mice within 10 weeks with minimum toxicity. Due to the iron doping and accumulation in the liver based on biodistribution studies, it is likely that the nanoshells are cleared via hepatic clearance. Since nanoshells are hollow, 3 times more silica nanoshells compared to solid particles can be injected for equal dosage based on mg/kg [57].

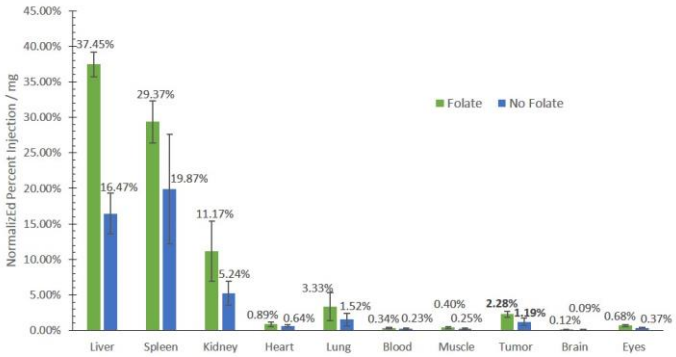

Figure 4. Biodistribution of folate functionalized nanoshells and non-folate functionalized nanoshells 5 days after IV injection. The normalized percent was determined by percent radiation normalized to total injection and normalized to tissue weight.

Ultrasound Imaging Mechanism. *In vitro* ultrasound experiments were performed on liquid PFP filled 500 nm silica nanoshell particles and observed by TEM (JEOL 1200 EX II) at different ultrasound insonation pressures in order to elucidate the ultrasound imaging mechanism (Figure 5) of the silica nanoshell particles.

0278-0062 (c) 2017 IEEE. Personal use is permitted, but republication/redistribution requires IEEE permission. See http://www.ieee.org/publications_standards/publications/rights/index.html for more information.

This article has been accepted for publication in a future issue of this journal, but has not been fully edited. Content may change prior to final publication. Citation information: DOI 10.1109/TMI.2017.2740784, IEEE Transactions on Medical Imaging

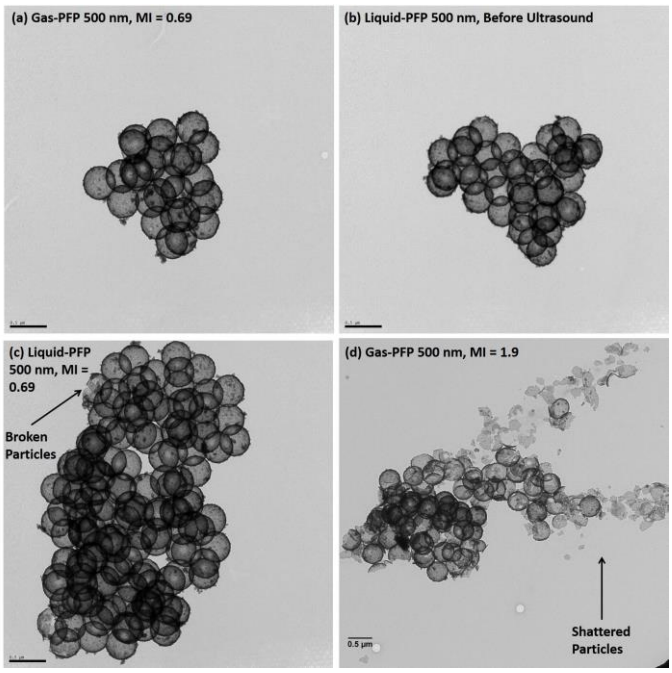

Figure 5. TEM of nanoshells in different regimes. (a) Gas-PFP filled 500 nm nanoshells exposed to low ultrasound power, MI = 0.69 (1.83 MPa). (b) Liquid-PFP filled 500 nm nanoshells before ultrasound insonation. (c) Liquid-PFP filled 500 nm nanoshells exposed to low ultrasound power at MI = 0.69 (1.83 MPa) for 24 hours. (d) Liquid PFP filled 500 nm nanoshells exposed to high ultrasound power at MI = 1.9 (5.03 MPa) for 24 hours. The population of shattered nanoshells are pointed out with the black arrows.

At high ultrasound power (MI = 1.9, 5.03 MPa), the Doppler ultrasound signal persisted for 24 hours of continuous imaging before completely extinguishing. TEM showed that 43.4 % of the nanoshells were shattered. This is consistent with the strong ultrasound signal originating from inertial cavitation that fragmented the nanoshells at high ultrasound power (Figure 5 and Supplemental Figure 2). In contrast, liquid PFP filled 500 nm silica nanoshells were exposed to low ultrasound power (MI = 0.69, 1.83 MPa) for 24 hours. Under TEM, nanoshells exposed to low ultrasound power appears identical to nanoshells that were not exposed to any ultrasound insonation.

Table 1. Nanoshell shattering percentage at different regimes. Statistical analysis of liquid PFP filled 500 nm particles exposed to different ultrasound power regimes. Note that small holes are defined as holes with diameters less than 0.5 um. There were no shattered nanoshells before ultrasound exposure and after low ultrasound insonation (MI = 0.69). A total of 5343 particles were counted for the statistical measurement including at least 1100 for each category of particle collected from over several TEM images.

	Before Ultrasound	MI = 0.69 (Gas PFP)	MI = 0.69 (Liquid PFP)	MI = 1.9 (Liquid PFP)
Broken	0.16%	0.36%	0.35%	43.40%

IV. Conclusion

It has been shown that the 500 nm hard shell Fe (III) doped silica nanoshells are a strong ultrasound contrast agent with a long *in vivo* lifetime and are retained by tumors, which allows continued ultrasound imaging using CPS and SPSI. Their small size and ease of surface modification allows for accumulation or enhanced retention at the tumor site with passive targeting by the EPR effect and folate conjugation appears to mainly lead to increased retention at the tumor site after EPR accumulation. The hard shell silica nanoparticles minimized PFP diffusion from the shell to the bloodstream and enhanced stability in tissue, which resulted in long *in vivo* imaging lifetimes. In addition, the nanoshells were sufficiently fragile to be shattered with a single high intensity ultrasound pulse, which provides a new on demand imaging modality, SPSI. After IV injection in the mouse tail vein, the particles were observed by SPSI to accumulate in the implanted tumor up to a mean of 3.3 ± 1 days post injection while not interfering with conventional diagnostic ultrasound imaging. Adding folate surface functionalization extended the *in vivo* SPSI imaging lifetime by a factor of four to a mean of 12 ± 2 days post injection. While functionalization is often thought to have a minimal effect in delivering large nanoparticles to tumors [51], here, the functionalization results in enhanced nanoparticle retention by the tumor. In contrast to the long lived *in vivo* ultrasound imaging attained in the present work, current clinically approved microbubble contrast agents exhibit an *in vivo* lifetime of less than thirty minutes [27, 28]. SPSI in conjunction with the long-lived silica based ultrasound contrast agents represent a new class of ultrasonic imaging tools that can be applied to tumor localization and monitoring. Receptor-specific surface modification may further provide the important function of probing for molecular expressions in the tumor microenvironment [58-60] as well as localized drug delivery applications [61]. The ultra-long lifetime enables ultrasound molecular imaging of early stage tumor development with biomarkers.

Acknowledgment: NIH grant support 1R33CA177449, NIH-NCI-NCTC-R21T, NIH fellowship support (James Wang, Natalie Mendez), 1F31CA177199 (Casey Ta) and corporate support, from Samsung and Siemens-Philips are gratefully acknowledged.

References

[1] E. Stride and N. Saffari, "Microbubble ultrasound contrast agents: a review," *Proceedings of the Institution of Mechanical Engineers, Part H: Journal of Engineering in Medicine,* vol. 217, pp. 429-447, 2003.

[2] B. B. Goldberg, J.-B. Liu, and F. Forsberg, "Ultrasound contrast agents: a review," *Ultrasound in medicine & biology,* vol. 20, pp. 319-333, 1994.

[3] R. E. Kerber, J. M. Kioschos, and R. M. Lauer, "Use of an ultrasonic contrast method in the diagnosis of valvular regurgitation and intracardiac shunts," *The American journal of cardiology,* vol. 34, pp. 722-727, 1974.

0278-0062 (c) 2017 IEEE. Personal use is permitted, but republication/redistribution requires IEEE permission. See http://www.ieee.org/publications_standards/publications/rights/index.html for more information.

This article has been accepted for publication in a future issue of this journal, but has not been fully edited. Content may change prior to final publication. Citation information: DOI 10.1109/TMI.2017.2740784, IEEE Transactions on Medical Imaging

[4] D. Cosgrove, "Ultrasound contrast agents: an overview," *European journal of radiology,* vol. 60, pp. 324-330, 2006.

[5] N. De Jong, F. Ten Cate, C. Lancee, J. Roelandt, and N. Bom, "Principles and recent developments in ultrasound contrast agents," *Ultrasonics,* vol. 29, pp. 324-330, 1991.

[6] F. Forsberg, D. Merton, J. Liu, L. Needleman, and B. Goldberg, "Clinical applications of ultrasound contrast agents," *Ultrasonics,* vol. 36, pp. 695-701, 1998.

[7] F. Kiessling, S. Fokong, P. Koczera, W. Lederle, and T. Lammers, "Ultrasound microbubbles for molecular diagnosis, therapy, and theranostics," *J Nucl Med,* vol. 53, pp. 345-8, Mar 2012.

[8] R. Gramiak and P. M. Shah, "Echocardiography of the aortic root," *Investigative radiology,* vol. 3, pp. 356-366, 1968.

[9] R. Gramiak, P. M. Shah, and D. H. Kramer, "Ultrasound cardiography: contrast studies in anatomy and function," *Radiology,* vol. 92, pp. 939-948, 1969.

[10] S. H. Bloch, M. Wan, P. A. Dayton, and K. W. Ferrara, "Optical observation of lipid-and polymer-shelled ultrasound microbubble contrast agents," *Applied Physics Letters,* vol. 84, pp. 631-633, 2004.

[11] S. Garg, A. A. Thomas, and M. A. Borden, "The effect of lipid monolayer in-plane rigidity on< i> in vivo</i> microbubble circulation persistence," *Biomaterials,* vol. 34, pp. 6862-6870, 2013.

[12] E. G. Schutt, D. H. Klein, R. M. Mattrey, and J. G. Riess, "Injectable microbubbles as contrast agents for diagnostic ultrasound imaging: the key role of perfluorochemicals," *Angewandte Chemie International Edition,* vol. 42, pp. 3218-3235, 2003.

[13] A. Raisinghani and A. N. DeMaria, "Physical principles of microbubble ultrasound contrast agents," *The American journal of cardiology,* vol. 90, pp. 3-7, 2002.

[14] A. Kabalnov, D. Klein, T. Pelura, E. Schutt, and J. Weers, "Dissolution of multicomponent microbubbles in the bloodstream: 1. Theory," *Ultrasound in medicine & biology,* vol. 24, pp. 739-749, 1998.

[15] T. Yasu, G. W. Schmid-Schönbein, B. Cotter, and A. N. DeMaria, "Flow dynamics of QW7437, a new dodecafluoropentane ultrasound contrast agent, in the microcirculation: microvascular mechanisms for persistent tissue echo enhancement," *Journal of the American College of Cardiology,* vol. 34, pp. 578-586, 1999.

[16] H. P. Martinez, Y. Kono, S. L. Blair, S. Sandoval, J. Wang-Rodriguez, R. F. Mattrey*, et al.*, "Hard shell gas-filled contrast enhancement particles for colour Doppler ultrasound imaging of tumors," *Medchemcomm,* vol. 1, pp. 266-270, 2010.

[17] A. Liberman, H. P. Martinez, C. N. Ta, C. V. Barback, R. F. Mattrey, Y. Kono*, et al.*, "Hollow silica and silica-boron nano/microparticles for contrast-enhanced ultrasound to detect small tumors," *Biomaterials,* vol. 33, pp. 5124-5129, 2012.

[18] K. K. Pohaku Mitchell, A. Liberman, A. C. Kummel, and W. C. Trogler, "Iron (III)-doped, silica nanoshells: a biodegradable form of silica," *Journal of the American Chemical Society,* vol. 134, pp. 13997-14003, 2012.

[19] A. Liberman, N. Mendez, W. C. Trogler, and A. C. Kummel, "Synthesis and surface functionalization of silica nanoparticles for nanomedicine," *Surface Science Reports,* vol. 69, pp. 132-158, 2014.

[20] A. H. Lo, O. D. Kripfgans, P. L. Carson, E. D. Rothman, and J. B. Fowlkes, "Acoustic droplet vaporization threshold: effects of pulse duration and contrast agent," *Ultrasonics, Ferroelectrics and Frequency Control, IEEE Transactions on,* vol. 54, pp. 933-946, 2007.

[21] O. D. Kripfgans, J. B. Fowlkes, D. L. Miller, O. P. Eldevik, and P. L. Carson, "Acoustic droplet vaporization for therapeutic and diagnostic applications," *Ultrasound in medicine & biology,* vol. 26, pp. 1177-1189, 2000.

[22] M. L. Fabiilli, K. J. Haworth, N. H. Fakhri, O. D. Kripfgans, P. L. Carson, and J. B. Fowlkes, "The role of inertial cavitation in acoustic droplet vaporization," *Ultrasonics, Ferroelectrics and Frequency Control, IEEE Transactions on,* vol. 56, pp. 1006-1017, 2009.

[23] O. D. Kripfgans, J. B. Fowlkes, M. Woydt, O. P. Eldevik, and P. L. Carson, "In vivo droplet vaporization for occlusion therapy and phase aberration correction," *Ultrasonics, Ferroelectrics and Frequency Control, IEEE Transactions on,* vol. 49, pp. 726-738, 2002.

[24] M. Zhang, M. L. Fabiilli, K. J. Haworth, F. Padilla, S. D. Swanson, O. D. Kripfgans*, et al.*, "Acoustic droplet vaporization for enhancement of

0278-0062 (c) 2017 IEEE. Personal use is permitted, but republication/redistribution requires IEEE permission. See http://www.ieee.org/publications_standards/publications/rights/index.html for more information.

This article has been accepted for publication in a future issue of this journal, but has not been fully edited. Content may change prior to final publication. Citation information: DOI 10.1109/TMI.2017.2740784, IEEE Transactions on Medical Imaging

thermal ablation by high intensity focused ultrasound," *Academic radiology,* vol. 18, pp. 1123-1132, 2011.

[25] X. Wang, H. Chen, Y. Chen, M. Ma, K. Zhang, F. Li*, et al.*, "Perfluorohexane-Encapsulated Mesoporous Silica Nanocapsules as Enhancement Agents for Highly Efficient High Intensity Focused Ultrasound (HIFU)," *Advanced Materials,* vol. 24, pp. 785-791, 2012.

[26] P. S. Sheeran, V. P. Wong, S. Luois, R. J. McFarland, W. D. Ross, S. Feingold*, et al.*, "Decafluorobutane as a phase-change contrast agent for low-energy extravascular ultrasonic imaging," *Ultrasound in medicine & biology,* vol. 37, pp. 1518-1530, 2011.

[27] A. L. Klibanov, "Ligand-carrying gas-filled microbubbles: ultrasound contrast agents for targeted molecular imaging," *Bioconjugate chemistry,* vol. 16, pp. 9-17, 2005.

[28] S. Qin, C. F. Caskey, and K. W. Ferrara, "Ultrasound contrast microbubbles in imaging and therapy: physical principles and engineering," *Physics in medicine and biology,* vol. 54, p. R27, 2009.

[29] A. Liberman, J. Wang, N. Lu, R. D. Viveros, C. Allen, R. Mattrey*, et al.*, "Mechanically Tunable Hollow Silica Ultrathin Nanoshells for Ultrasound Contrast Agents," *Advanced Functional Materials,* 2015.

[30] J. S. Horoszewicz, S. S. Leong, E. Kawinski, J. P. Karr, H. Rosenthal, T. M. Chu*, et al.*, "LNCaP model of human prostatic carcinoma," *Cancer research,* vol. 43, pp. 1809-1818, 1983.

[31] P. F. Bousquet, M. F. Braña, D. Conlon, K. M. Fitzgerald, D. Perron, C. Cocchiaro*, et al.*, "Preclinical evaluation of LU 79553: a novel bis-naphthalimide with potent antitumor activity," *Cancer research,* vol. 55, pp. 1176-1180, 1995.

[32] A. Faustino-Rocha, P. A. Oliveira, J. Pinho-Oliveira, C. Teixeira-Guedes, R. Soares-Maia, R. G. Da Costa*, et al.*, "Estimation of rat mammary tumor volume using caliper and ultrasonography measurements," *Lab animal,* vol. 42, p. 217, 2013.

[33] T. L. Szabo, *Diagnostic ultrasound imaging: inside out*: Academic Press, 2004.

[34] A. Liberman, Z. Wu, C. V. Barback, R. Viveros, S. L. Blair, L. G. Ellies*, et al.*, "Color Doppler ultrasound and gamma imaging of intratumorally injected 500 nm iron–silica nanoshells," *ACS nano,* vol. 7, pp. 6367-6377, 2013.

[35] A. Liberman, Z. Wu, C. V. Barback, R. D. Viveros, J. Wang, L. G. Ellies*, et al.*, "Hollow iron-silica nanoshells for enhanced high intensity focused ultrasound," *Journal of Surgical Research,* 2014.

[36] H. Hashizume, P. Baluk, S. Morikawa, J. W. McLean, G. Thurston, S. Roberge*, et al.*, "Openings between defective endothelial cells explain tumor vessel leakiness," *The American journal of pathology,* vol. 156, pp. 1363-1380, 2000.

[37] M. K. Danquah, X. A. Zhang, and R. I. Mahato, "Extravasation of polymeric nanomedicines across tumor vasculature," *Advanced drug delivery reviews,* vol. 63, pp. 623-639, 2011.

[38] Y. Nakamura, A. Mochida, P. L. Choyke, and H. Kobayashi, "Nanodrug Delivery: Is the Enhanced Permeability and Retention Effect Sufficient for Curing Cancer?," *Bioconjugate Chemistry,* vol. 27, pp. 2225-2238, 2016.

[39] F. Yuan, M. Dellian, D. Fukumura, M. Leunig, D. A. Berk, V. P. Torchilin*, et al.*, "Vascular permeability in a human tumor xenograft: molecular size dependence and cutoff size," *Cancer research,* vol. 55, pp. 3752-3756, 1995.

[40] S. K. Hobbs, W. L. Monsky, F. Yuan, W. G. Roberts, L. Griffith, V. P. Torchilin*, et al.*, "Regulation of transport pathways in tumor vessels: role of tumor type and microenvironment," *Proceedings of the National Academy of Sciences,* vol. 95, pp. 4607-4612, 1998.

[41] R. K. Jain, "Transport of molecules, particles, and cells in solid tumors," *Annual review of biomedical engineering,* vol. 1, pp. 241-263, 1999.

[42] R. K. Jain and T. Stylianopoulos, "Delivering nanomedicine to solid tumors," *Nature reviews Clinical oncology,* vol. 7, pp. 653-664, 2010.

[43] A. Moore, E. Marecos, A. Bogdanov Jr, and R. Weissleder, "Tumoral distribution of long-circulating dextran-coated iron oxide nanoparticles in a rodent model 1," *Radiology,* vol. 214, pp. 568-574, 2000.

[44] J. T. Pinto, B. P. Suffoletto, T. M. Berzin, C. H. Qiao, S. Lin, W. P. Tong*, et al.*, "Prostate-specific membrane antigen: a novel folate hydrolase in human prostatic carcinoma cells," *Clinical Cancer Research,* vol. 2, pp. 1445-1451, 1996.

0278-0062 (c) 2017 IEEE. Personal use is permitted, but republication/redistribution requires IEEE permission. See http://www.ieee.org/publications_standards/publications/rights/index.html for more information.

This article has been accepted for publication in a future issue of this journal, but has not been fully edited. Content may change prior to final publication. Citation information: DOI 10.1109/TMI.2017.2740784, IEEE Transactions on Medical Imaging

[45] A. Ghosh and W. D. Heston, "Tumor target prostate specific membrane antigen (PSMA) and its regulation in prostate cancer," *Journal of cellular biochemistry,* vol. 91, pp. 528-539, 2004.

[46] Y. Hattori and Y. Maitani, "Enhanced in vitro DNA transfection efficiency by novel folate-linked nanoparticles in human prostate cancer and oral cancer," *Journal of controlled release,* vol. 97, pp. 173-183, 2004.

[47] W. Xia, A. R. Hilgenbrink, E. L. Matteson, M. B. Lockwood, J.-X. Cheng, and P. S. Low, "A functional folate receptor is induced during macrophage activation and can be used to target drugs to activated macrophages," *Blood,* vol. 113, pp. 438-446, 2009.

[48] I. Hilgendorf and F. K. Swirski, "Folate Receptor: A Macrophage “Achilles' Heel”?," *Journal of the American Heart Association,* vol. 1, p. e004036, 2012.

[49] C. P. Wong, T. M. Bray, and E. Ho, "Induction of proinflammatory response in prostate cancer epithelial cells by activated macrophages," *Cancer letters,* vol. 276, pp. 38-46, 2009.

[50] N. Kamaly, Z. Xiao, P. M. Valencia, A. F. Radovic-Moreno, and O. C. Farokhzad, "Targeted polymeric therapeutic nanoparticles: design, development and clinical translation," *Chemical Society Reviews,* vol. 41, pp. 2971-3010, 2012.

[51] S. Acharya and S. K. Sahoo, "PLGA nanoparticles containing various anticancer agents and tumour delivery by EPR effect," *Advanced drug delivery reviews,* vol. 63, pp. 170-183, 2011.

[52] R. Weissleder, M. Nahrendorf, and M. J. Pittet, "Imaging macrophages with nanoparticles," *Nature materials,* vol. 13, pp. 125-138, 2014.

[53] R. Kumar, I. Roy, T. Y. Ohulchanskky, L. A. Vathy, E. J. Bergey, M. Sajjad*, et al.*, "In vivo biodistribution and clearance studies using multimodal organically modified silica nanoparticles," *ACS nano,* vol. 4, pp. 699-708, 2010.

[54] G. Xie, J. Sun, G. Zhong, L. Shi, and D. Zhang, "Biodistribution and toxicity of intravenously administered silica nanoparticles in mice," *Archives of toxicology,* vol. 84, pp. 183-190, 2010.

[55] B. Godin, C. Chiappini, S. Srinivasan, J. F. Alexander, K. Yokoi, M. Ferrari*, et al.*, "Discoidal porous silicon particles: fabrication and biodistribution in breast cancer bearing mice," *Advanced functional materials,* vol. 22, pp. 4225-4235, 2012.

[56] X. He, H. Nie, K. Wang, W. Tan, X. Wu, and P. Zhang, "In vivo study of biodistribution and urinary excretion of surface-modified silica nanoparticles," *Analytical chemistry,* vol. 80, pp. 9597-9603, 2008.

[57] N. Mendez, A. Liberman, J. Corbeil, C. Barback, R. Viveros, J. Wang*, et al.*, "Assessment of in vivo systemic toxicity and biodistribution of iron-doped silica nanoshells," *Nanomedicine: Nanotechnology, Biology and Medicine,* vol. 13, pp. 933-942, 2017.

[58] F. Chen, H. Hong, S. Shi, S. Goel, H. F. Valdovinos, R. Hernandez*, et al.*, "Engineering of hollow mesoporous silica nanoparticles for remarkably enhanced tumor active targeting efficacy," *Scientific reports,* vol. 4, 2014.

[59] J. K. Willmann, N. van Bruggen, L. M. Dinkelborg, and S. S. Gambhir, "Molecular imaging in drug development," *Nature Reviews Drug Discovery,* vol. 7, pp. 591-607, 2008.

[60] J. L. Vivero-Escoto, R. C. Huxford-Phillips, and W. Lin, "Silica-based nanoprobes for biomedical imaging and theranostic applications," *Chemical Society Reviews,* vol. 41, pp. 2673-2685, 2012.

[61] M. Liong, J. Lu, M. Kovochich, T. Xia, S. G. Ruehm, A. E. Nel*, et al.*, "Multifunctional inorganic nanoparticles for imaging, targeting, and drug delivery," *ACS nano,* vol. 2, pp. 889-896, 2008.

0278-0062 (c) 2017 IEEE. Personal use is permitted, but republication/redistribution requires IEEE permission. See http://www.ieee.org/publications_standards/publications/rights/index.html for more information.